# NANOSTRUCTURED THERMAL PROTECTION SYSTEMS FOR SPACE EXPLORATION MISSIONS

SECOND INTERNATIONAL PROBE WORKSHOP
NASA AMES RESEARCH CENTER, MOFFETT FIELD, CA
AUGUST 23-26, 2004

**J. O. Arnold[(1)], Y.K. Chen[(2)], T. Squire[(2)], D. Srivastava[(1)],G. Allen, Jr[(3)], M. Stackpoole[(3)], H. E. Goldstein[(4)], E. Venkatapathy[(2)] and M. P. Loomis[(2)]**

*[(1)]NACNT, University Affiliated Research Center, Moffett Field, CA 94035, USA jarnold@mail.arc.nasa.gov, deepak@nas.nasa.gov*
*[(2)]NASA Ames Research Center, Moffett Field, CA 94035, ykchen@mail.arc.nasa.gov, tsquire@mail.arc.nasa.gov, evenkatapathy@mail.arc.nasa.gov, mloomis@mail.arc.nasa.gov*
*[(3)]Eloret Corporation, Ames Research Center, Moffett Field, CA 94035, gallen@mail.arc.nasa.gov, mstackpoole@mail.arc.nasa.gov*
*[(4)]Consultant, Ames Research Center, Moffett Field, CA 94305, hgoldstein@mail.arc.nasa.gov*

## ABSTRACT

Strong research and development programs in nanotechnology and Thermal Protection Systems (TPS) exist at NASA Ames. Conceptual studies have been undertaken to determine if new, nanostructured materials (composites of existing TPS materials and nanostructured composite fibers) could improve the performance of TPS. To this end, we have studied various candidate heatshields, some composed of existing TPS materials (with known material properties), to provide a baseline for comparison with others that are admixtures of such materials and a nanostructured material. In the latter case, some assumptions were made about the thermal conductivity and strength of the admixture, relative to the baseline TPS material. For the purposes of this study, we have made the conservative assumption that only a small fraction of the remarkable properties of carbon nanotubes (for example) will be realized in the material properties of the admixtures employing them. The heatshields studied included those for Sharp leading edges (appropriate to out-of-orbit entry and aero-maneuvering), probes, an out-of-orbit Apollo Command Module (as a surrogate for NASA's new Crew Exploration Vehicle [CEV]), a Mars Sample Return Vehicle and a large heat shield for Mars aerocapture missions. We report on these conceptual studies, which show that in some cases (not all), significant improvements in the TPS can be achieved through the use of nanostructured materials.

## 1. INTRODUCTION

Carbon nanotube (CNT)-based materials have the potential to revolutionize the design of future aerospace vehicles. As discussed in [1], CNTs exhibit Young's modulus of over 1 Tera Pascal, and tensile strength of about 200 Giga Pascal. They are about hundred times stronger than steel at 1/6th its weight. CNTs have thermal conductivities on the order of 3000 W/m$^{o}$K in the axial direction - seven times higher than the thermal conductivity of copper. Perpendicular to this direction, the thermal conductivity is (0.25 W/m$^{o}$K), essentially that of an insulator. Carbon nanotube materials can also be electrical conductors, semiconductors or insulators and can have piezoelectrical properties suitable for very high force activators. Composites made of CNTs and other nanostructured materials may benefit from these remarkable properties.

The low thermal conductivity in directions normal to the fiber and the high temperature stability when protected from oxidizing environments make them ideal candidates for both ablative and blanket-based heat shields. The high axial thermal conductivity of CNTs allows their use as passive heat pipes, transporting heat from hot spots on thermal shields to cooler areas, improving heat shield performance and reducing weight. Herein we analyze various cases of interest for future human and robotic space exploration missions, to evaluate benefits that could flow from incorporating nanostructured TPS materials. For our study, we have not assumed that the admixtures in which the nanomaterials are embedded will be endowed with the same remarkable material properties exhibited, for instance, in pure, single wall carbon nanotubes. Instead, we have made conservative assumptions about the level of enhancement that might reasonably be expected in the material properties of the admixtures, relative to those of baseline TPS materials.

## 2.0 VEHICLES ENTERING EARTH'S ATMOSPHERE

### 2.1 Vehicle with Sharp Leading Edges

The first application we considered was for vehicles with sharp leading edges (Fig. 1). As explained in

[2,3], such high Lift/Drag vehicles provide good aerodynamic performance, giving wide cross range capabilities, valuable for out-of-Earth-orbit missions. Such vehicles also offer value to aerogravity assist missions for solar exploration at Venus, for example, or for targeting the placement of nano- or micro-probes to Jupiter, cases where rapid deployment of assets such as orbiters and probes is needed.

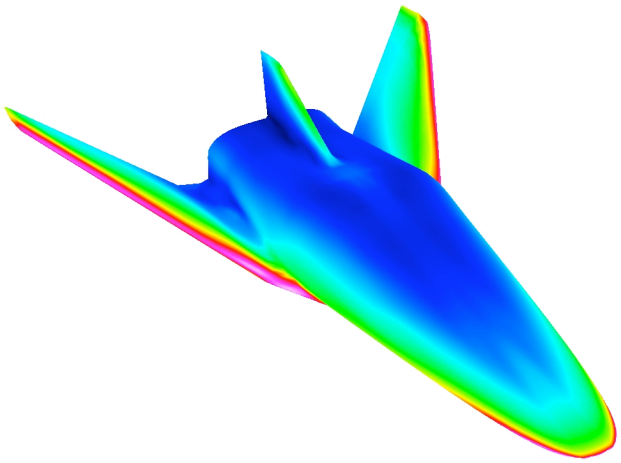

*Fig. 1 Proposed highly maneuverable hypervelocity, out-of-Earth-orbit vehicle [3], known as SHARP V-5.*

Fig. 2 shows the 2-D coupled thermal/stress model of a wing leading edge that was developed [4] as a part of efforts conducted at Ames during the second Reusable Launch Vehicle Program. The UHTC is made of $HfB_2$ (20 volume percent SiC). This leading edge is attached to an SiC structured wing fixture. Research [4] demonstrated that a 2-D thermo-structural model can reliably predict 3-D performance for this configuration.

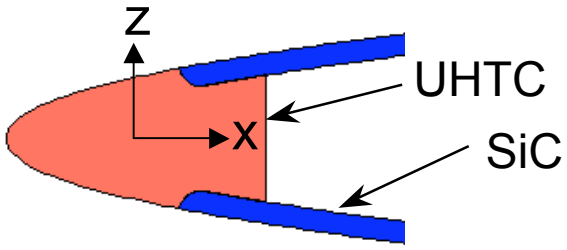


*Fig 2. Representation of the nose of a Sharp leading edge vehicle.*

Fig. 3 displays the flight conditions for the sharp leading edge depicted in Fig. 2. The initial time (t = 0) corresponds to the atmospheric pierce point altitude of 122 km. This trajectory was designed to minimize the integrated heat load. Heating was predicted with real-gas Computational Fluid Dynamics (CFD) codes. Note that the wing leading edge flew at an angle of attack of $35^0$ for a little more than 20 minutes and then dropped rapidly to $15^0$. Since the wing was at angle of attack, the heating is not symmetrical.

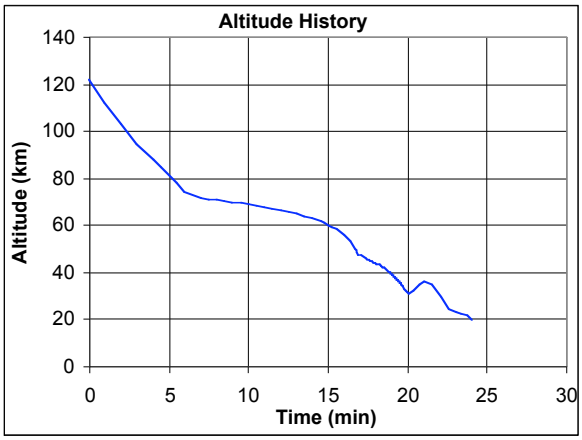


Fig. 3 (a) Altitude-time history.

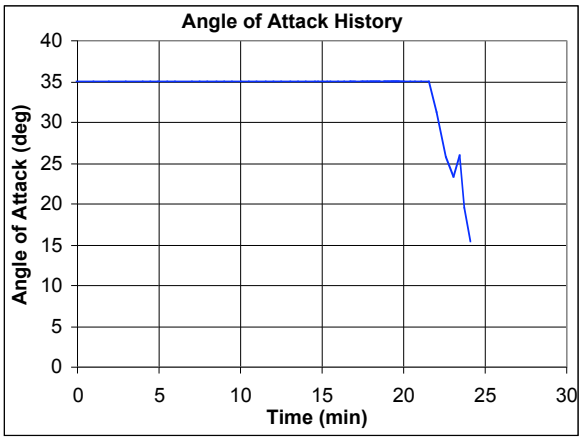


Fig. 3(b) Angle-of-attack history.

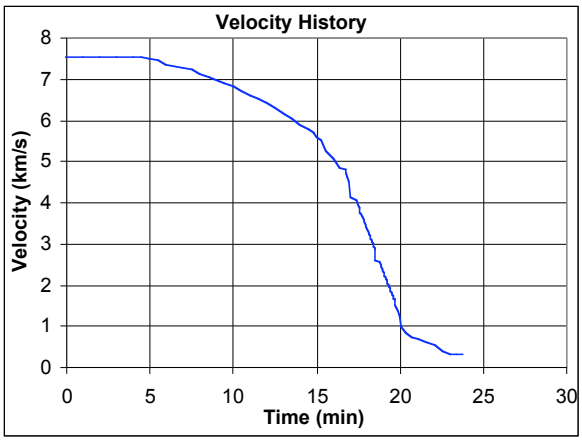


Fig. 3(c) Velocity History

In order to explore how nanotechnology could improve the performance of UHTC Sharp leading edges, two cases were considered. The first (nominal) case considered the UHTC $HfB_2/SiC$, using its established thermal conductivity and assuming it to be isotropic. The second case considered a UHTC/nanostructured admixture, assumed to have, in the X direction (Fig. 2), twice the thermal conductivity of $HfB_2/SiC$ and in the Z direction, the same thermal conductivity as HfB2/SiC. The increased thermal conductivity in the X direction for such an admixture might be accomplished by fibers containing nanotubes (possibly CNTs) laid up with their axes in the X direction. The assumed value of twice the nominal thermal conductivity is far lower than that for pure CNTs, and allows for imperfect phonon transport in composite fibers. Fig. 4 shows the thermal conductivity for both cases as a function of temperature. It was assumed in both cases that there is no change in the isotropic mechanical properties of the UHTC.

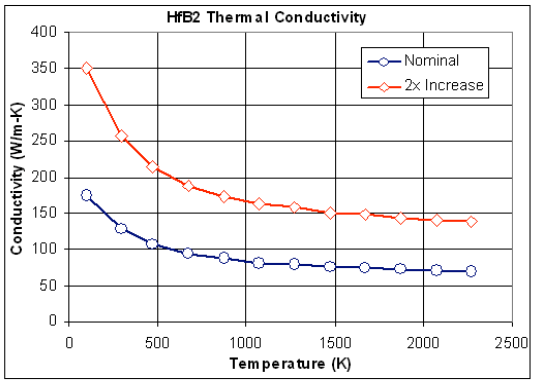


*Fig. 4. Thermal conductivity as a function of temperature.*

Fig. 5(a) shows the results of the thermal analysis for three key locations on the sharp leading edge, located by the circles in Fig. 5(b). The bold curves represent the nominal case, with the isotropic thermal conductivity, while the thin curves represent the case where this property is doubled in the X-direction.

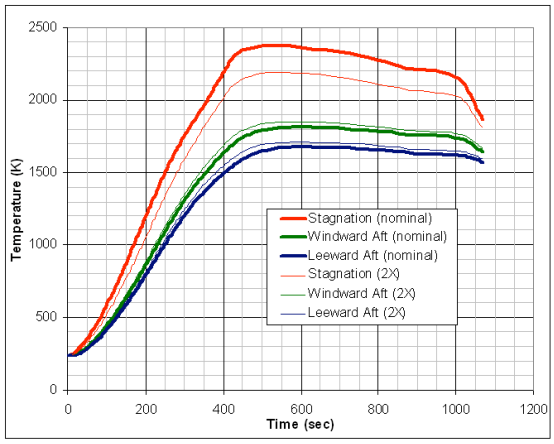


*Fig. 5(a): Temperature profiles for locations circled in Fig. 5(b).*

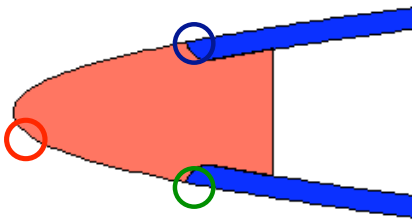

*Fig. 5(b). Circles indicate three key locations on the sharp UHTC leading edge plotted in Fig. 5(a).*

The airfoil is at a positive angle of attack, so the stagnation point is on the lower edge, and the leeward attachment to the SiC structure runs cooler than that on windward side. It is important to note that the case with heterogeneous thermal conductivity results in a drop in the peak temperature at the stagnation point of 182 $^0$K (328 $^0$F). Such a reduction would make the UHTC less likely to oxidize and would increase the lifetime and reusability of the leading edge material. It is also noteworthy that the temperature (38$^0$K or 68$^0$F) at the UHTC/SiC attachment points is only slightly higher for case 2 than for the nominal case, suggesting that the assembly is viable for both cases.

We believe that the reason for all these changes in temperature is the 'passive heat pipe effect', arising from the increased thermal conductivity in the X-direction. With this effect, the equilibrium radiation from the sides of the UHTC effectively cools the stagnation point and the surrounding material.

Fig. 6 (a) is a plot of the principal stress history in the middle of the UHTC leading edge, the location of which is indicated by the circle in Fig. 6(b). Note that there is a very significant reduction in the tensile stress for the nanostructured material: doubling the thermal

conductivity in the X-direction reduces the peak interior stress from 51.4 Mpa to 32.8 Mpa, a decrease of 36 percent.

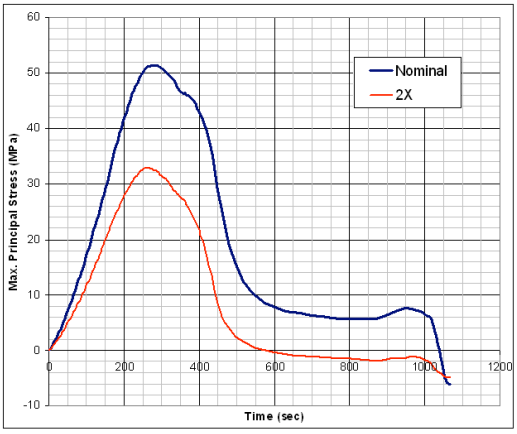


*Fig. 6(a). Principal tensile stress in the UHTC leading edge versus time.*

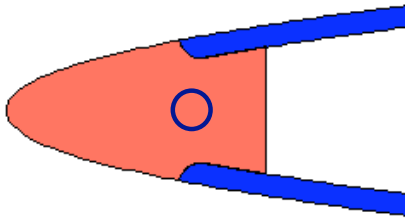

*Fig. 6(b). Location of principal tensile stress in UHTC leading edge.*

Future-generation materials for use on space transportation vehicles of the type described above require substantial improvements in material properties, leading to increased reliability and safety. UHTCs composed primarily of metal diborides are candidate materials for sharp leading edges on hypersonic re-entry vehicles. It is yet to be determined if they possess the properties necessary to withstand the extreme environments experienced at the leading edges during re-entry without undergoing some recession, oxidation or thermal shock. The design and processing of aligned nanotube-reinforced composites (composed of UHTC-type matrices with nanotube reinforcements) studied herein promises enhanced performance. It is hoped that, because of the extremely high thermal conductivity of the nanotubes, the overall thermal conductivity of the nanotube-reinforced UHTC system will show an increase over that of the baseline system, and yield increased performance. The conceptual study above offers considerable encouragement that the use of nanostructured materials will produce improvements.

If designed and processed correctly, we believe nanotube-reinforced UHTC composites could lead to a system with higher thermal conductivity than that found in the base UHTC material. These nanotube-reinforced composites could potentially dissipate heat away from localized regions of the leading edge and enable vehicles with leading edge geometries that provide improved performance and greater cross range. The drop in temperature at these localized regions may be sufficient to eliminate recession in these systems and allow for a reusable system. As part of this study, not shown here, there were indications that this approach may also yield improvements in other material properties, including toughness and thermal shock resistance, and so offer performance superior to that of current materials proposed for sharp leading edge applications. This approach may also yield composites that fail in a more graceful manner than current UHTC systems.

Initial samples comprising of aligned nanotubes in a refractory matrix have been processed. Preliminary mechanical properties and microscopy confirm that a preferred alignment has been achieved in them.

### 2.2 Out-of-Earth-orbit crewed vehicle (Apollo Command Module as a surrogate Crew Exploration Vehicle)

NASA's new vision for Space Exploration features the development of a Crew Exploration Vehicle (CEV) that would be used progressively for (1) out-of-orbit flight demonstrations, (2) Lunar Return missions and eventually, (3) return of astronauts from Mars. The precept of "spiral development" has been deemed appropriate for the CEV, giving rise to the opportunity to design a multi-use vehicle with a heatshield that is replaceable and able to be upgraded with a higher performance TPS when new missions demand it or when it becomes available. No concepts for the CEV have yet been developed by NASA's Office of Exploration (OExP), so we chose the Apollo Command Module as a surrogate CEV shape, and evaluated a nano-TPS for it.

Other studies ongoing [5] at Ames suggest that multifunctional approaches to the TPS for the CEV could result in significant mass savings. These concepts involve the use of a low-molecular-weight TPS, able to serve triple duty as Thermal, Radiation and Impact Protective Shields (TRIPS). This work suggests that fully dense Carbon Phenolic (CP) or lower density versions of CP would be good candidates as a starting points for TRIPS. Our study therefore concerns the potential benefits of using Carbon Phenolic as part of a nano-structured TPS for an Apollo Command Module shaped CEV.

At present, we have only analyzed the Apollo AS 202 out-of-orbit case. Wright, Prabhu and Martinez recently published [6] heat flux contours for this flight using a modern real-gas CDF code (DPLR). While their work was focused on afterbody flows, their forebody heat flux distribution is useful for our needs, and has been adopted herein. Fig. 7 shows the geometry of the Apollo vehicle used in [6].

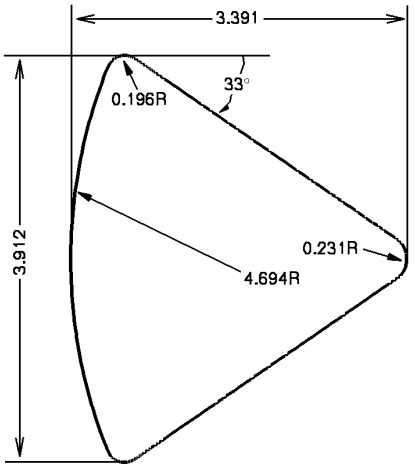


*Fig. 7. Schematic drawing of the outer mold line of the AS-202 Apollo Command Module used in [6].*

Fig. 8 (based on the work in [6], and provided to the present authors), displays the heat flux contours for Apollo AS 202 at the peak heating conditions, at a speed of 7.8 km/sec and an angle of attack of $18^{O}$. The stagnation point is on the lower (windward) edge of the figure.

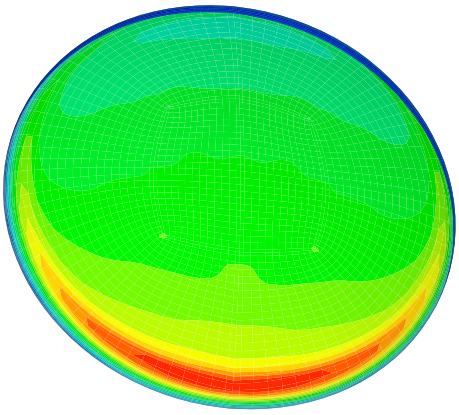

*Fig. 8. Heat flux contours for the Apollo AS 202 flight at peak heating conditions from [6]. The stagnation point is on the lower edge of the figure.*

Fig. 9 displays the heat flux distribution along the plane of symmetry passing through the stagnation point for the Apollo AS 202 flight at the peak heating conditions specified above, and for the heat flux contours shown in Fig. 8. The peak heat flux at the stagnation point is slightly more than 100 W/cm$^2$ and falls to a value near 40 W/cm$^2$ on the leeward edge of the forebody.

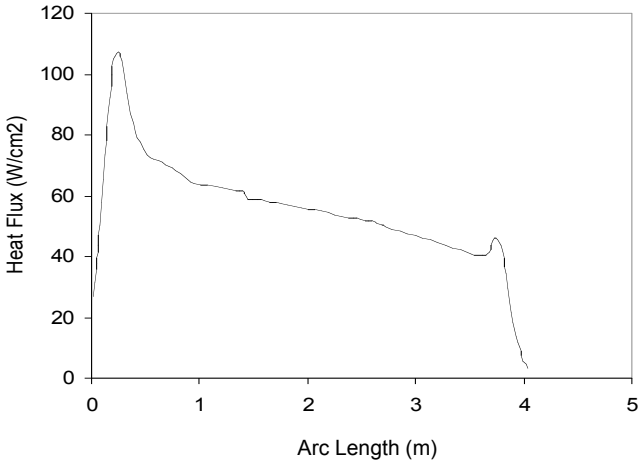


*Fig. 9. Computed heat flux distribution in the plane of symmetry for the Apollo AS 202 flight at peak heating conditions from [6], corresponding to Fig 8. The origin of the streamline distance is the windward side edge or the forebody.*

Fig. 10, predicted by the BLIMP program [7], displays the normalized stagnation point history of AS-202.

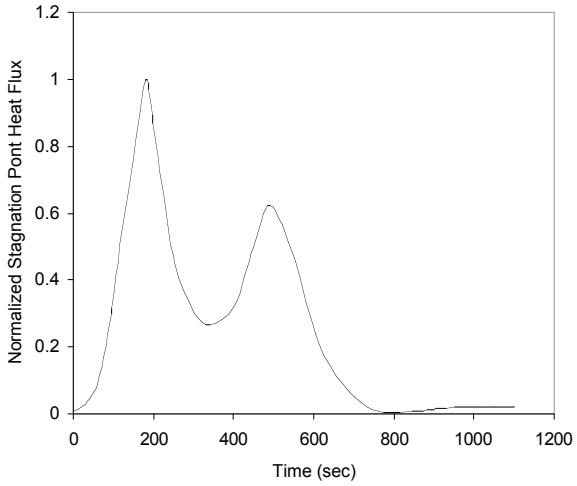


*Fig. 10. Normalized stagnation point heating history for Apollo Command module for flight AS-202 computed with the code from [7].*

Figs. 11 and 12 display the results of our calculations along the plane of symmetry, using the TITAN Code

[8]. The calculations are 2-D for the boundary conditions corresponding to the distributions in Figs 8 and 9.

Two cases were considered: (1) a heat shield made of fully dense Carbon Phenolic, whose properties are given in [9], and (2), a heatshield made of an admixture of fully dense CP and carbon nanotube composite fibers. For case 1, the thickness of the CP to sustain the bond line temperature at 250 $^{O}$C was 4.65 cm. Fig. 11 shows the history of the stagnation point temperature while that for the bondline at the stagnation point is shown in Fig. 12. Splash down occurs at about 1100 seconds. Maintaining the bondline temperature at 250 $^{O}$C or less at splashdown is the primary TPS requirement.

The material properties for the second case (95% CP + 5% nano-fiber by volume) are assumed to be identical to those for pure CP, except that the thermal conductivity of the admixture along the plane of symmetry is 500 W/m$^{0}$K, higher than the value for pure fully dense CP at 0.55 W/m$^{0}$K. As Fig.11 shows, the addition of carbon nanotube fibers has no effect on the stagnation point temperature history. There is a reduction of about 30$^{0}$C in the bondline temperature at the stagnation point in case 2, compared to case 1. This reduction illustrates the passive heat pipe effect: a migration of heat from the hot stagnation point region to the cooler, downstream portion of the heat shield. It is estimated that this effect results is an overall saving of 5-10% in the heat shield mass.

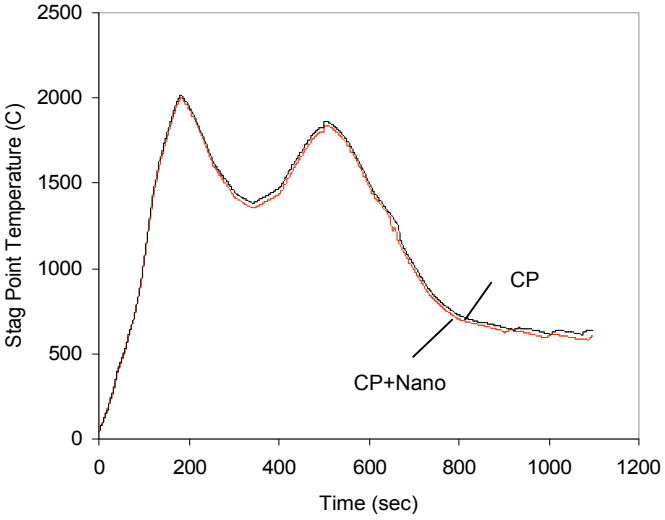


*Fig. 11. TITAN [8] solutions for the stagnation point temperature history for the AS 202 trajectory and heating rate profile shown in Figs. 10 and 11.*

While this effect is not as large as we had hoped for, it does illustrate that nanostructured TPS could be useful for improved designs for heat shields. One improvement could be in safety margins for bondline temperatures and another could be for specialized cooling of local "hot spots" like those areas where cavity heating may occur, such as the strut mounting locations commonly used for support of probes in launch stacks. As our colleagues at Ames extend their CFD study to the higher speed cases (e.g., Apollo 4 at Lunar Return speeds), we will continue our conceptual studies to look for benefits in these cases.

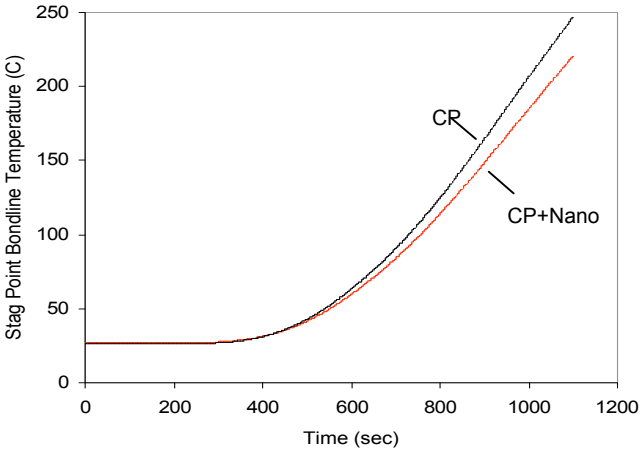


*Fig. 12. TITAN solutions for the bondline temperature history for the AS 202 trajectory and heating rate profile shown in Figs 9 and 10. The prime TPS requirement is that the bondline temperature does not exceed 250 $^{0}$C.*

### 2.3 Sample Return Mission

Two NASA missions to return samples to Earth are currently underway: Genesis and Stardust [10,11]. Genesis will return (in September 2004) samples of solar wind material expelled from the Sun; Stardust will return ejecta from Comet Wild 2, in January 2006. Both spacecraft will enter the Earth's atmosphere at hyperbolic return speeds. These missions represent the beginning of a concerted effort to understand the Solar System by returning samples recovered from deep space to the Earth for detailed scientific study.

The entry system we chose to analyze is a generic sample return capsule (SRC) similar to the proposed Mars Sample Return (MSR) Earth Entry Vehicle (EEV) [12]. Because of the possibility of returning a biohazard from Mars, the MSR EEV TPS system is required to have a probability of failure of one in a million or less. CP was chosen for the TPS material on the MSR EEV because of its widespread use in ballistic missile nose tip applications and for the Pioneer-Venus and Galileo atmospheric probes [13, 14].

Fig. 13 depicts the entry of the MSR EEV, which will occur at speeds ranging from slightly above Lunar Return (11 km/sec) to as high as 13 km/sec, depending upon the trans Mars-Earth trajectory chosen. The sample is contained in an inner sphere, inside a crushable, insulated outer sphere behind the CP heat shield, as shown in the cut-away in Fig. 13.

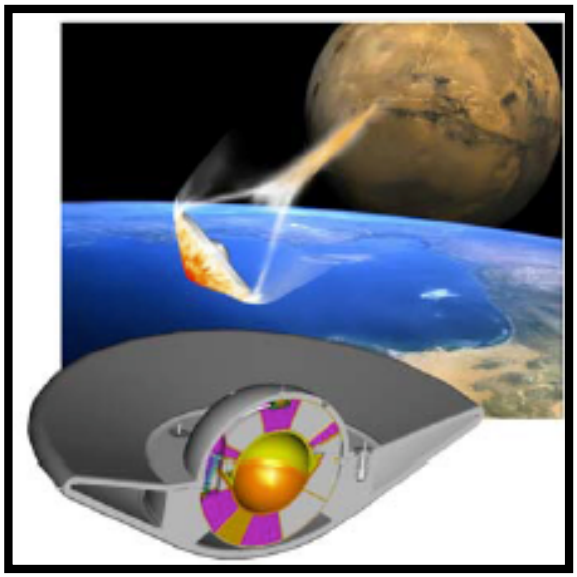

*Fig. 13. Artist's concept of the MSR EEV. Courtesy of J. Corliss, Langley Research Center.*

Since we saw a reduction of only 5-10% in heat shield mass during our study of nanostructured CP for the surrogate CEV study, we decided to explore nanostructured Reinforced Carbon-Carbon (RCC) - a thermostructural TPS - for a vehicle of the same general configuration as the MSR EEV. RCC has been quite successfully used on the wing leading edges of the Space Shuttle.

Fig. 14 depicts the cross-sectional view of a Sample Return Capsule (SRC) fitted with a 6.35 mm thick RCC forebody heat shield comprised of a 0.9 m base diameter, blunted $60^0$ half-angle cone. The base diameter of the SRC RCC forebody is the same as that for the MSR EEV studied in [12]. We stress that the purpose here is to study options for a generic SRC, and not advocate an alternate MSR EEV vehicle.

As for the UHTC study in section 2.1, we carried out calculations of the thermal response to the Earth entry for two cases: (1) RCC with accepted values of its material properties provided by D. Curry of the Johnson Space Center [15], and (2) a nano-structured modification of RCC, whose thermal conductivity is assumed to be homogenously double that of RCC. Fig. 15 (a) depicts the heat flux as a function of time at the stagnation point of the RCC forebody. The entry speed was 11.5 km/sec and the heating was computed using TITAN, a state-of-the-art code [8]. Fig. 15 (b) displays the resulting temperature histories as a function of time for key locations at the centerline.

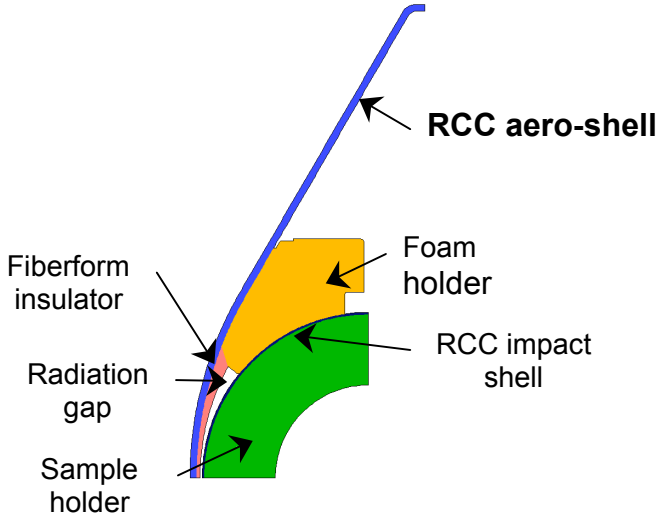


*Fig. 14. Axisymmetric cross-section of an SRC, similar to the MSR EEV in [12], except that it is fitted with a Reinforced Carbon-Carbon heat shield. This is intended to be a generic SRC, not advocated here as a replacement of the MSR EEV.*

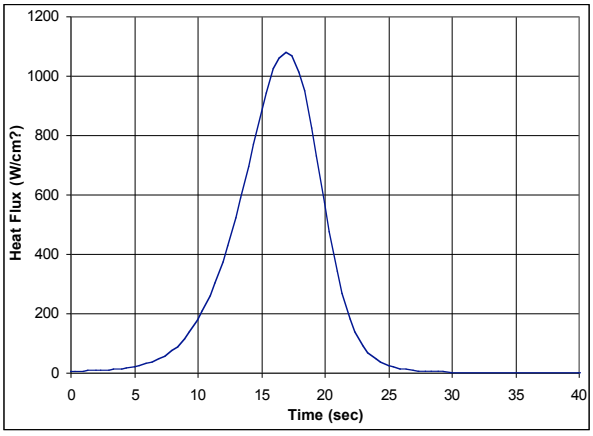


*Fig. 15(a) Heat flux ($W/cm^2$) Versus Time (sec) for the SRC Entering the Earth's Atmosphere at 11.5 km/sec.*

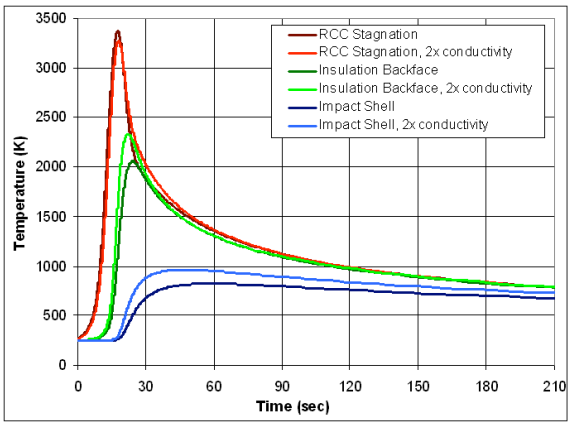


*Fig. 15(b). Temperature history at the centerline of the SRC, resulting from the heating from the environment shown in Fig. 15 (b).*

The results of the calculations for cases (1) and (2) indicated that the peak tensile stress, located at the juncture of the RCC and the Fiberform insulator, was 228 Mpa, beyond the typical in-plane tensile strengths for RCC, which range from 50–300 MPa. Stress maps for both cases were similar, and it appeared to the authors that the attachment of a thin RCC aeroshell to the substructure could be a major design issue for the RCC forebody.

However, it should be pointed out that yet another property of nanostructured materials could remedy this problem. Estimates by one of us (D.S.), using standard micromechanics models, suggest that tensile strengths of 1 to 2 GPa could be achieved in a nanostructured RCC with an admixture of 90 percent RCC/10 percent carbon nanotube composite and, if so, the issue would be resolved.

It is significant to note that if one could achieve these results, the mass reduction of the nanostructured RCC SRC compared to the MSR EEV baseline, would be 14 kg, a 32 percent total entry mass savings. This mass savings can be understood by comparing the cross sectional views in Figs. 13 and 14. Note that much of the supporting structure for the CP in Fig. 13 is eliminated by use of an RCC forebody in Fig. 14, and this is the source of much of the mass savings.

We are aware that the "open" appearance of the SRC afterbody might cause concern from an aerodynamics/heating perspective, but private communications [16] suggest the CFD for this should be achievable with modern codes and hoped-for flight validation experiments.

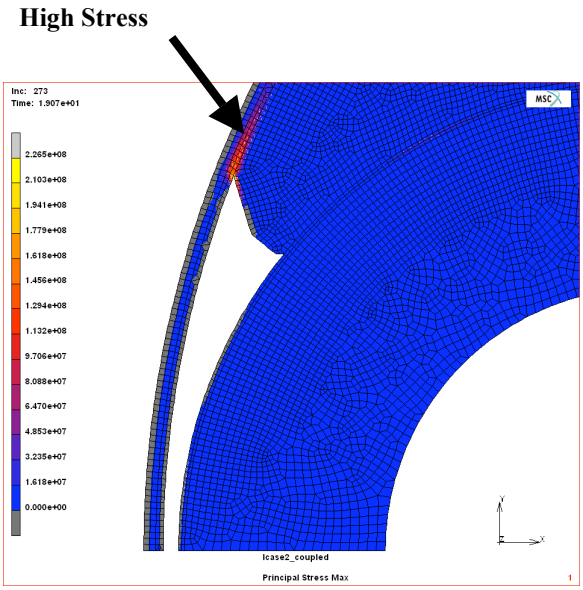


*Figure 16. Stress diagram for axisymmetric SRC. Note that the high area of stress is at the attachment point where the forebody and underlying fiberform structure are joined.*

## 3.0 MARS HUMAN AEROCAPTURE VEHICLE

NASA's new Space Exploration Program includes the goal of implementing a human Mars mission. Again, no mission planning for this mission is yet available from the OExP.

During the decade of the 1990's, Johnson Space Center led NASA's development of detailed Reference Missions for the Human Exploration of Mars [17]. These studies clearly showed that mass lifted into low Earth Orbit (LEO) is the principal metric to be minimized for affordable Human Mars Exploration Missions. Aerocapture, and subsequent out-of-orbit descent to the surface of Mars was identified as a "winner" for mass reduction regardless of the propulsion system used for the trans-Earth to Mars trajectory insertion (chemical, nuclear or solar electric). The studies pioneered the multifunctional use of structures as a mass-saving tool. For example, the shroud of the launch vehicle for Earth surface to LEO, containing the Mars exploration systems, doubled as the Mars aeroshell of the aerocapture/descent vehicle. Three of the current authors (J.A., Y.K.C and E.V.) participated in those studies along with others from Ames Research Center, and we adopt herein their results carried out for the JSC-led mission analysis.

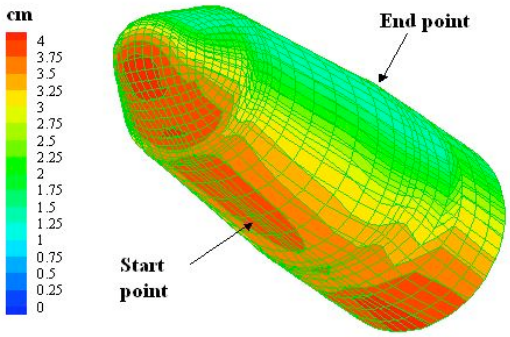


*Fig. 17. Perspective view of the 28 meter long human Mars aerocapture vehicle from[17]. The bar indicates the local heat shield thickness in cm.*

Fig. 17 shows a perspective of the Human Mars Aerocapture vehicle with a TPS thickness map, optimized for the vehicle encapsulated in a lightweight material, Silcone Impregnated Reusable Ceramic Ablator (SIRCA) [9]. The bar specifies TPS thickness in cm. Fig. 18 displays the stagnation point heat flux history for the aerocapture maneuver. As seen, the heat flux reaches almost 300 W/cm$^2$ during the maneuver. The primary constraint for the TPS sizing is that the bond line at any location does not exceed 250 $^{O}$C. Fig. 19 displays the heating distribution along the streamline distance (represented by S), connecting the points labeled "start point" and "end point", respectively, in Fig 17. The reference length, L is 11.5 m and the start point is in the plane of symmetry.

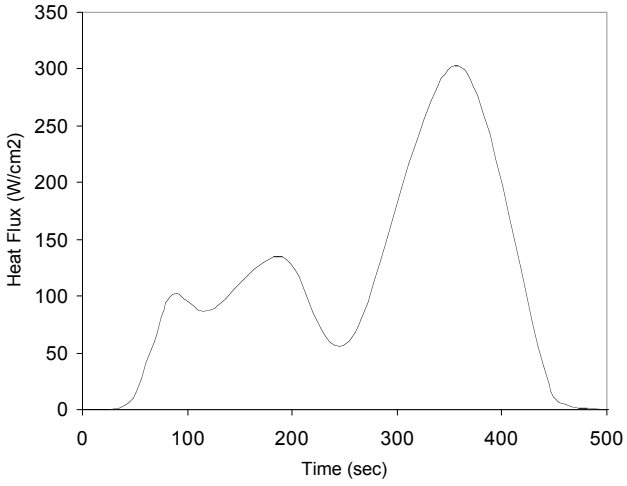


*Fig. 18. Heat flux history during aerocapture at the stagnation point discussed above and in [17].*

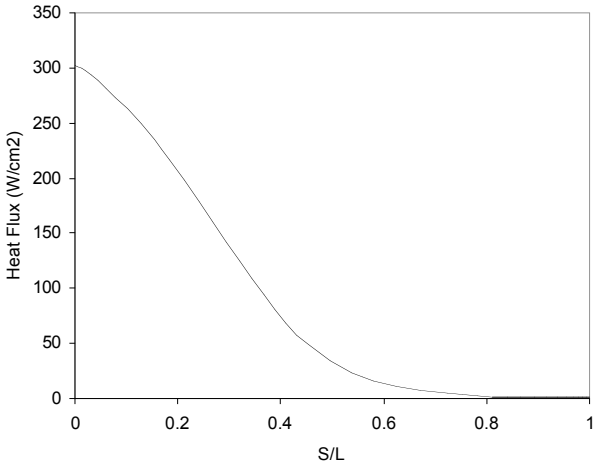


*Fig. 19. Heating distributions along the streamline whose start and end points are shown in Fig. 17.*

Fig. 20 is a plot of the percentage reduction in thickness from the SIRCA TPS thickness achieved by replacing the pure SIRCA with a 95% SIRCA-5% carbon nanotube admixture. The carbon nanotube fibers were assumed to be aligned along the streamline coordinate S/L. For pure SIRCA, the thermal conductivity at room temperature is 0.06 W/m$^{O}$K, while that for the admixture at room temperature is 480 W/m$^{O}$K.

This calculation was performed with the TITAN code [8] and the thermal conductivity is a function of temperature. As the plot shows, there are significant computed percentage reductions in local TPS thickness along the streamline on the windward (hot) side of the heat shield, but there is an increase in thickness on the windward (cool) afterbody region. The average thickness reduction over the streamline is only 0.98 percent, which is small. However, if there is a hot spot reasonably close to a minimum TPS thickness, the passive heat pipe effect might still be used to decrease the total TPS weight significantly. We note that if the carbon nanotube fibers were affixed to a heat sink, e.g. a conformal water tank for human life support, the TPS mass reductions could even be more significant. The carbon nanotube fibers could facilitate such a design, but the required system study is beyond the scope of the present paper.

## SUMMARY AND CONCLUDING REMARKS

We have reported herein the results of conceptual studies to explore some of the benefits that might flow from the emerging field of nanotechnology, by improving TPS performance for missions of continuing interest to NASA. In particular, these studies are intended to suggest areas that might be appropriate for further study. We stress that the material properties of

the nanostructured materials adopted in the studies are conjectural, but might be achieved through considerable research and development efforts.

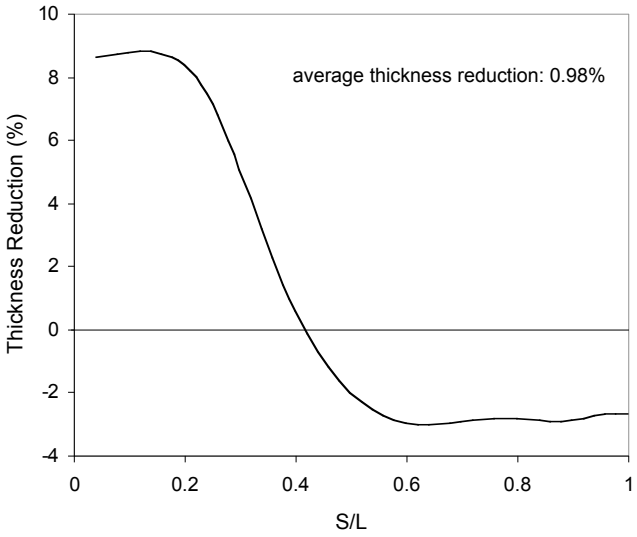


*Fig. 20. Plot of predicted local TPS thickness reductions along a streamline connecting the start and endpoints specified in Fig. 17.*

With these cautions noted, our conceptual studies indicate the following:

• UHTC properties may be modified by nanostructuring thermal conductivity, improving resistance to oxygen attack and thermal shock resistance. Such materials would find applications in aerogravity assist missions and for high L/D out-of-Earth-orbit vehicles, capable of greater cross range capabilities than vehicles with blunter leading edges.

• The passive heat pipe effect provided by nanostructured materials admixed with standard CP and SIRCA heat shield materials modestly improves TPS performance for an Apollo-type CEV and the Human Mars Aerocapture Vehicles. Passive heat piping, where aeroheating is delivered to heat sinks (e.g. water tanks on human vehicles), could provide good system design options, but an estimation of the benefits from this approach was beyond the scope of the present study.

• Our studies suggest that a significant portion (32 percent) of the total entry mass of a Sample Return vehicle could be achieved through the use of a nanostructured RCC thermostructural heat shield. This would be achieved by the increased tensile strength that may be afforded by carbon nanostructured materials.

**ACKNOWLEDEGMENTS**

The authors gratefully acknowledge that our efforts were enabled by funding from Ames Internal Research and Development program under the aegis of the Center's Strategic Research Council. J.A. acknowledges support under grant NAG2-1580 SC 20030034. J.A. and D.S acknowledge support under UARC Task Order T0.014.0.HP.IN, Contract NAS2-3144. The authors appreciate the efforts by Mary Gage in preparing the manuscript.

**REFERENCES**

[1] Meyyappan, M. and Srivastava, D., Handbook for Nanoscience, Engineering and Technology, Chaper18, CRC Press 2003, Editors: Goddard, W. III, and Brenner, D., Lyshevskik, S., and Iafrate, G.

[2] Arnold, J. O., Johnson, S. M. and Wercinski, P. F., "SHARP: NASA's Research and Development Activities in Ultra High Temperature Ceramic Nose Caps and Leading Edges for Future Space Transportation Vehicles", Paper IAF-01-V5.02, IAF Symposium, Toulouse France, October 1-5, 2001

[3] Reuther, J., Kinney, D., Smith, S., Kontinos, D., Saunders, D, and Gage, P., "A Reusable Space Vehicle Design Study Exploring Sharp Leading Edges, AIAA Conference Paper 2001-2884, June 2001.

[4] MSC.Marc Nonlinear Finite Element Solver, MSC.Software Corporation, 260 Sheridan Ave., Suite 309, Palo Alto, CA 94306 (www.marc.com).

[5] Loomis, M. P, and Arnold, J. O., "Thermal, Radiation and Impact Protective Shields (TRIPS) For Robotic and Human Space Exploration Missions", 2nd International Planetary Probe Workshop NASA Ames Research Center, Moffett Field, CA August 23-27, 2004.

[6] Wright, M. J., Prabhu, D. K., and Martinez, E. R., "Analysis of Afterbody Heating Rates on the Apollo Command Modules, Part I; AS-202". 37th AIAA Thermophysics Conference, Portland OR, AIAA Paper 2004-2456.

[7] Bartlett, E. P, Abett, M. J., Nicolet, W. E., and Moyer, C. B. "Improved Heat-Shield Design Procedures for Manned Entry Systems, Part II: Application to Apollo". Contract NAS9-9494, June 22, 1970, Aerotherm Corporation.

[8] Chen, Y.K., and Milos, F. S., "Two-Dimensional Implicit Ablation Thermal Response and Ablation Program for Charring Materils on Hypersonic Space Vehicles", Journal of Spcecraft and Rockets, Vol 38, No. 4, 2001, pp 473-481.

[9][NASA Ames Web Site for TPSX]: http://tpsx.arc.nasa.gov/index.html

[10] NASA JPL Web Site for Genesis: http://genesismission.jpl.nasa.gov

[11] NASA JPL Web Site for Stardust: http://stzrdust.jpl.nasa.gov

[12] Mitcheltree, R., Hughes, S. R. Dillman and Teler, J., “An Earth Entry Vehicle for Returning Samples from Mars”, AAAF paper ARVS-102, Second Atmospheric Reentry Vehicles and Systems, March 26-29, Arachon, France.
[13] Fimmel, R. O., Colin, L. and Burgess, E. NASA SP-461, “Pioneer Venus”, 1983.
[14] Milos, F.S., "Galileo Probe Heat Shield Ablation Experiment," Journal of Spacecraft and Rockets, Vol. 34, No. 6, 1997, pp. 705-713 and Milos, F.S., Chen, Y.K., Squire, T. H. and Brewer, R.A., "Analysis of Galileo Probe Heatshield Ablation and Temperature Data," Journal of Spacecraft and Rockets, Vol. 36, No. 3, 1999, pp. 298-306.
[15] Curry, D. private communication, July 2004, Properties of Reinforced Carbon-Carbon.
[16] Wright, Michael J. Private Communication, July 2004.
[17] Bret, D., Editor: “Reference Mission 3.0 Addendum to the Human Exploration of Mars: The Reference Mission of the NASA Mars Exploration Study Team”. JSC June, 1998.
http://ares.jsc.nasa.gov/HumanExplore/Exploration/EXLibrary/docs/MarsRef/contents.html